PHYSICAL REVIEW B **78**, 180414(R) (2008)

Direct observation of the spin structures of vortex domain walls in ferromagnetic nanowires

T. Nagai,[1,2,*] H. Yamada,[3] M. Konoto,[3] T. Arima,[4] M. Kawasaki,[3,5] K. Kimoto,[2] Y. Matsui,[2] and Y. Tokura[1,3,6]
[1]*Multiferroics Project, ERATO, JST, c/o FRS-CMRG, RIKEN, Wako 351-0198, Japan*
[2]*Advanced Electron Microscopy Group, NIMS, Tsukuba 305-0044, Japan*
[3]*Correlated Electron Research Center, AIST, Tsukuba 305-8562, Japan*
[4]*Institute of Multidisciplinary Research for Advanced Materials, Tohoku University, Sendai 980-8577, Japan*
[5]*WPI Advanced Institute for Materials Research, Tohoku University, Sendai 980-8577, Japan*
[6]*Department of Applied Physics, University of Tokyo, Hongo, Tokyo 113-8656, Japan*
(Received 18 October 2008; published 20 November 2008)

The spin structures of vortex domain walls forming in a ferromagnetic $La_{0.6}Sr_{0.4}MnO_3$ nanowire have been directly observed using Lorentz microscopy. We visualized the in-plane anisotropic structures, which exhibited twofold rotational symmetry and revealed that the simultaneous reversal of the vortex chirality and the magnetization directions of separated domains occurs at all the pinning sites. The observations indicate that the chirality is determined by the magnetization directions and the magnetic anisotropy induced at the pinning sites.

DOI: 10.1103/PhysRevB.78.180414 PACS number(s): 75.60.Ch, 75.25.+z, 75.30.−m, 75.75.+a

Nanoscaled ferromagnets play a key role in the emerging technology of spintronics, which takes advantage of the quantum-mechanical property of spin for the realization of future nonvolatile, high-density, and high-speed magnetoelectronic devices. The spin structures of nanometer-sized materials are therefore currently the subject of intensive study. In particular, a considerable amount of interest has been generated by the current- and field-induced motion of magnetic domain walls in these materials.[1–5] In magnetic imaging experiments on nanoscaled materials, magnetic force microscopy (MFM),[1–3] Lorentz microscopy,[6–9] scanning electron microscopy with polarization analysis (SEMPA),[10,11] photoemission electron microscopy (PEEM),[4,12] etc. have been used so far. It has been confirmed by experiments using these methods that two types of domain walls are formed in a ferromagnetic nanowire: transverse walls and vortex walls.[1–3,7–10,12] Transverse walls have magnetization at the center of the wall perpendicular to the wire axis, whereas vortex walls have magnetization forming a vortex.[13] Vortex walls are expected to have four spin configurations corresponding to the different magnetization directions of separated domains: head to head (HH) and tail to tail (TT) and the chirality of the vortex: clockwise (CW) and counterclockwise (CCW). However, these fine spin structures have not yet been clearly observed. Moreover, the mechanism of chirality formation, which is of great importance, is still unknown. In this Rapid Communication, we report on the direct observation of vortex domain-wall structures. The observed results provide a key to revealing the mechanism of chirality formation. The intrinsic nature of vortex walls is proved to be responsible for determining the chirality.

We used Lorentz microscopy combined with phase retrieval based on the transport-of-intensity (TIE) technique[14,15] to observe the in-plane structures. The Lorentz images were observed using a Lorentz electron microscope (Hitachi HF-3000L) operated at 300 kV and equipped with a liquid-nitrogen-type cooling sample holder. The magnetization distribution in the specimen was calculated from the electron phases, which were retrieved using the intensity of three differently focused (underfocused, in-focus, and overfocused) Lorentz images. When applying this technique to a ferromagnetic nanowire, we must take into account the interference effect of the electron wave at the edge of the wire. It is well known that interference fringes called Fresnel fringes appear at the edge of a specimen in conventional TEM observation because a phase difference of the electron wave arises between the specimen and the surrounding vacuum. The phase shift is caused by the mean inner potential of the specimen and is proportional to the sum of the atomic scattering amplitude for electrons and inversely proportional to the unit-cell volume of the crystal. To suppress the Fresnel fringes, it is necessary to enclose the ferromagnetic wire with a nonferromagnetic material, the mean inner potential of which is equivalent to that of the wire. To realize such a TEM specimen, we used strongly correlated electron materials, which show a marked change in their magnetic properties upon a slight variation in their chemical composition. The materials used were ferromagnetic perovskite-type manganese oxide $La_{0.6}Sr_{0.4}MnO_3$ (LSMO) ($T_C \sim 340$ K) (Ref. 16) and antiferromagnetic perovskite-type iron oxide $La_{0.6}Sr_{0.4}FeO_3$ (LSFO) ($T_N \sim 320$ K).[17] First, we fabricated an epitaxial thin-film sample in which LSFO (100 nm)/LSMO (100 nm)/LSFO (100 nm) layers were grown on a $SrTiO_3$ (001) substrate by pulsed-laser deposition. TEM specimens were then fabricated by applying a focused ion beam (FIB) to the sample. In the TEM specimen [Fig. 1(a)], a ferromagnetic LSMO nanowire is sandwiched between two LSFO nanowires. The size of the LSMO wire is 10 μm long (along x), 40 nm thick (along y), and 100 nm wide (along z). The very similar scattering factors[18] and cell volumes of the two materials[17] result in little difference in their mean inner potential. In the Lorentz microscopy observation, the incident electron beam was projected onto the specimen along y. Alternating current (ac) demagnetization was performed to form domain walls in the nanowire by the application of an external alternating magnetic field with a maximum intensity of 450 Oe along x. The simulations were performed using the object oriented micromagnetic framework (OOMMF) micromagnetic simulator[19] based on the Landau-Lifshitz-Gilbert (LLG) equation with the following input parameters: saturation magnetization $M_s = 400 \times 10^3$ A/m,[20] exchange stiff-

 ©2008 The American Physical Society

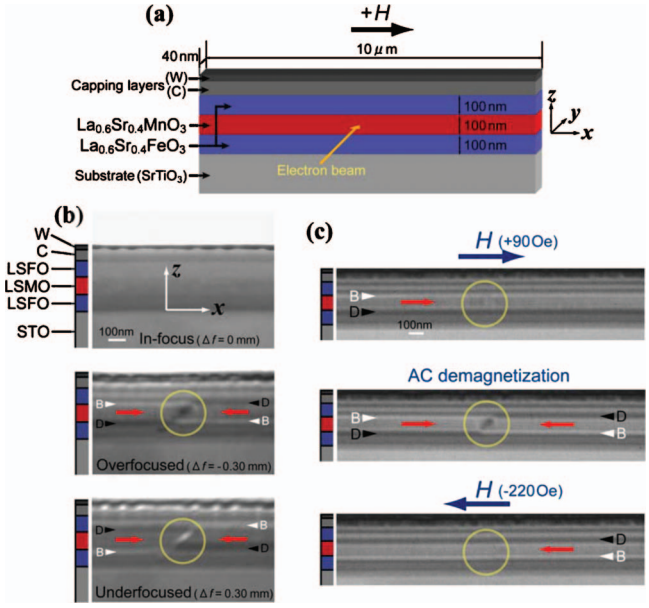

FIG. 1. (Color) Lorentz microscopy observations of a ferromagnetic LSMO nanowire. (a) Schematic illustration of a TEM specimen including a ferromagnetic LSMO nanowire sandwiched by two antiferromagnetic LSFO nanowires. The size of the LSMO nanowire is 10 μm (along x), $\times 40$ nm (along y), and $\times 100$ nm (along z). The directions of the external magnetic field and the electron beam are parallel to x and y, respectively. (b) A series of in-focus (top, $\Delta f=0$ mm), overfocused (middle, $\Delta f=-0.30$ mm), and underfocused (bottom, $\Delta f=0.30$ mm) Lorentz images taken at 80 K for the TEM specimen after ac demagnetization. (c) Variation in the magnetic contrast in the overfocused image upon applying a constant magnetic field along x. Whereas the middle image represents an initial magnetization state formed by ac demagnetization, the upper and lower images show the same area after applying magnetic fields of +90 and −220 Oe, respectively.

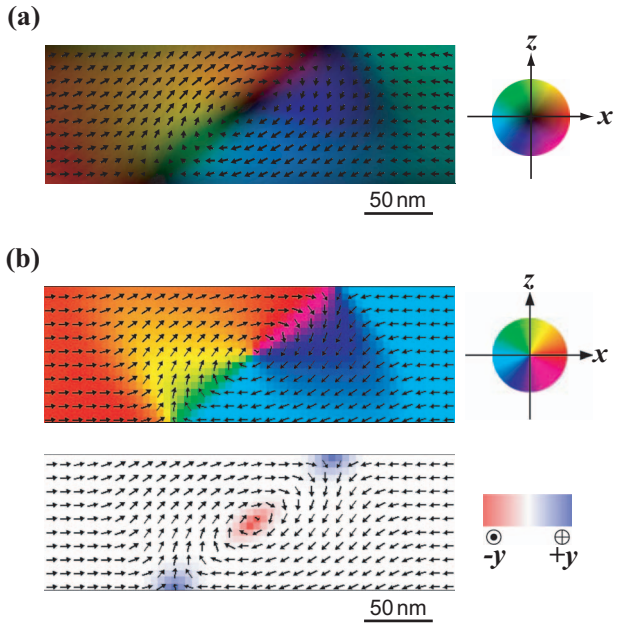

FIG. 2. (Color) In-plane magnetization distribution of a vortex domain wall in the LSMO nanowire. The size of the displayed area is 300×100 nm^2. (a) Distribution obtained by TIE analysis using the three images shown in Fig. 1(b). The black arrows and the color indicate the direction and intensity of the in-plane (x-z plane) component, respectively. (b) Distribution obtained by micromagnetic simulation based on the Landau-Lifshitz-Gilbert equation. The color in the upper figure represents the direction of the in-plane (x-z plane) component, and that in the lower figure represents the direction and intensity of the perpendicular (y) component; the arrows in both figures indicate the direction and intensity of the in-plane component.

ness $A=1.7\times 10^{-12}$ J/m,[21] and cell size of 5×10^{-9} m. Considering the structural property of the wire, an induced uniaxial anisotropy $K_u=8.4\times 10^3$ J/m^3 (Ref. 20) was assumed, as described below.

A set of Lorentz images observed after ac demagnetization at 80 K is shown in Fig. 1(b). By defocusing the objective lens, a magnetic contrast emerges in the image. In the overfocused image, a pair consisting of a bright line and a dark line (indicated by white and black triangles, respectively) appears in the vicinity of both edges of the LSMO nanowire. The positional relationship between the two lines on the left side of the dark oval-like area (enclosed by a circle) is opposite to that on the right side. The contrast of the lines and the oval-like area in the underfocused image is opposite to that in the overfocused image. The classical particlelike picture of electrons deflected by the Lorentz force in a magnetic field suggests that the corresponding area of the LSMO nanowire is composed of two domains with magnetization directions pointing toward each other, i.e., HH domains. To confirm the relationship between the magnetization directions and the linelike contrast, we investigated the variation in the magnetic contrast by applying a constant magnetic field [Fig. 1(c)]. The variation in the linelike contrast indicating the domain growth induced by the field is explained by the above relationship.

In Fig. 2(a) we display the in-plane magnetization distribution obtained by TIE analysis using the three images in Fig. 1(b). The magnetization structure of a HH-CW vortex domain wall can be clearly seen. The structure has twofold rotational symmetry about the center. In addition, the configuration has a striking feature: a band in which the magnetic moments rotate with a small radius. A Néel-wall-type area including the vortex core at the center is oriented diagonally across the wire, giving rise to anisotropy in the wall structure. The anisotropic configuration was well reproduced by the micromagnetic simulation, as shown in Fig. 2(b). The magnetization at the vortex core and both ends of the band has a significant perpendicular component. The directions of the component are opposite for the core and the ends. The component forms so as to avoid a large increase in the exchange energy. In accordance with this result, the experimentally observed intensity of the in-plane component markedly decreases at the core and the ends [Fig. 2(a)].

Figure 3 shows the results of TIE analysis using the Lorentz images for the entire configuration series of vortex domain walls: (a) HH-CW, (b) HH-CCW, (c) TT-CW, and (d) TT-CCW. The contrast of the walls in the images reflects the chirality. The aforementioned anisotropy is observed for every wall structure, as clearly shown in the bottom image for

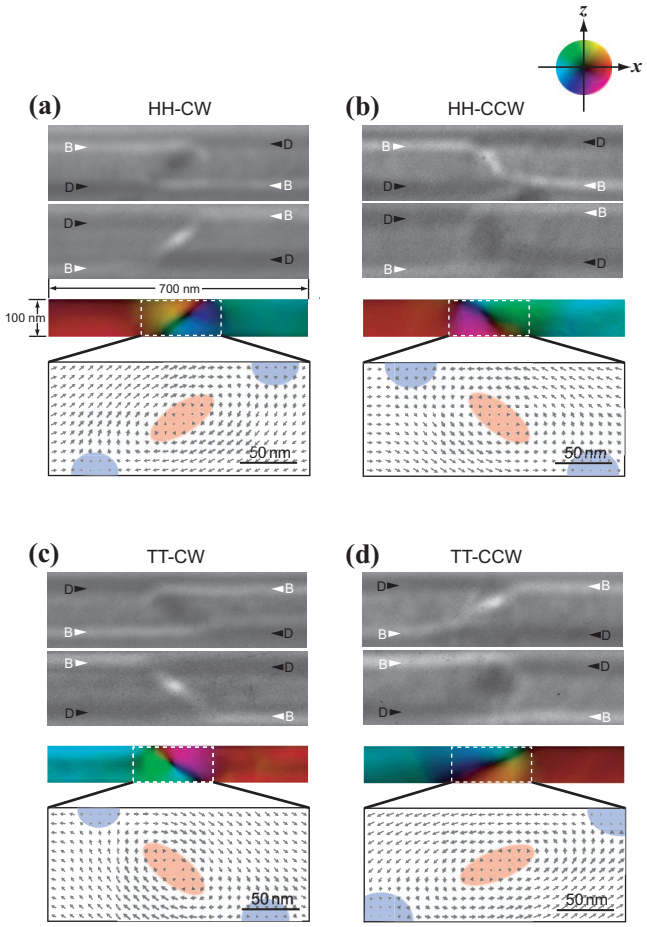

FIG. 3. (Color) TIE analyses for the entire configuration series of vortex domain walls. (a) HH-CW, (b) HH-CCW, (c) TT-CW, and (d) TT-CCW. Here, HH and TT stand for the head-to-head and tail-to-tail configurations of the magnetization, while CW and CCW for the clockwise and counterclockwise flow of the vortex, respectively. From top to bottom, an overfocused image ($\Delta f = -0.30$ mm), an underfocused image ($\Delta f = 0.30$ mm), the in-plane magnetization in the corresponding 700×100 nm^2 area, and the magnetization structure of the domain wall in a 230×100 nm^2 area are displayed for each vortex wall. In the colored areas in the bottom illustrations, the intensity of the in-plane component markedly decreases, suggesting the presence of an out-of-plane component. The micromagnetic simulations indicate that the directions of the perpendicular component are opposite for the red area (vortex core) and the blue area (end of the band).

each structure. However, it is noteworthy that the orientation of the band characterizing the anisotropy is dependent on the type of wall. Whether the band is oriented toward the top right or the top left is governed by two parameters: the magnetization directions of separated domains and the vortex chirality. The band is oriented toward the top right in HH-CW and TT-CCW vortex walls and toward the top left in HH-CCW and TT-CW vortex walls. In the colored areas, the intensity of the in-plane component markedly decreases, suggesting the presence of a perpendicular component. It is estimated from the micromagnetic simulations that the directions of the perpendicular component are opposite for the red area (vortex core) and the blue area (end of the band).

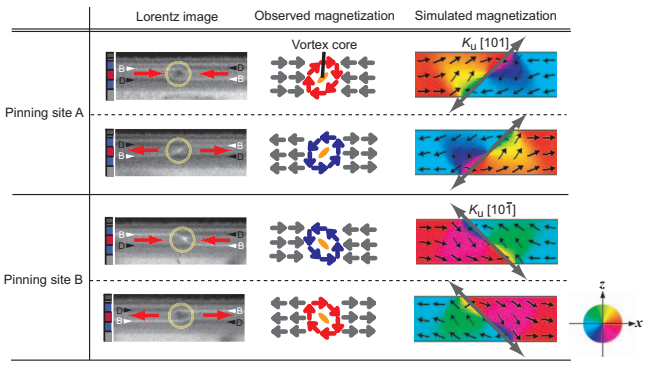

FIG. 4. (Color) Chirality reversal of vortex domain walls at two types of pinning sites A and B. Overfocused Lorentz images (left), observed magnetization (middle), and simulated magnetization (right) for vortex domain walls at pinning sites A and B are displayed. The simulation was performed under hypothetical anisotropy; the direction of the easy axis is [101] for site A and [10 −1] for site B. The upper and lower rows show the two different magnetization structures that form at each site. Only HH-CW and TT-CCW vortex walls form at site A, whereas only HH-CCW and TT-CW vortex walls do at site B. The simultaneous reversal of the vortex chirality and the magnetization directions of separated domains takes place at both sites.

We repeated the observation after carrying out ac demagnetization 100 times per specimen for a total of five specimens. We found that all the vortex walls were pinned at two to four specific positions in each specimen. For every pinning site, vortex walls pinned with the same magnetization directions of separated domains concomitantly have the same vortex chirality, indicating a freeze on the chiral degree of freedom. Moreover, the reversal of the vortex chirality and that of the magnetization directions of separated domains simultaneously occur at every pinning site. Two correlations exist between the vortex chirality and the magnetization directions when they are formed at the same time. All the pinning sites can be classified into two types according to the correlation, A and B, as shown in Fig. 4. Only HH-CW and TT-CCW vortex walls form at type-A sites, whereas only HH-CCW and TT-CW vortex walls do at type-B sites.

Neglecting the anisotropy energy, a CW vortex wall and a CCW vortex wall with the same magnetization directions of separated domains have the same formation energy. Micromagnetic simulations taking account of only magnetostatic and exchange energies showed that the two walls form with an equal probability. The result allows us to recognize that the anisotropy energy is different between the two walls in reality. It is well known that magnetic anisotropy can be induced by strain through magnetostriction.[22] In fact, our conventional TEM investigation revealed that a diffraction contrast caused by strain occurs near the areas corresponding to the pinning sites. To confirm the effect of strain-induced anisotropy on the chirality formation, we performed simulations taking the extrinsic anisotropy into account. The anisotropy was set to be uniaxial for simplicity and the induced easy axis was confined to the x-z plane. The simulations showed that the chiral degree of freedom is frozen, namely, only one of the two chirality forms always appears. It also

unraveled the correlation between the vortex chirality and the magnetization directions of separated domains; the correlation that occurs is dependent on the direction of the easy axis (Fig. 4). If the axis is oriented toward the top right in Fig. 1(a), i.e., the direction is between [100] and [001], the vortex walls that form at pinning site A are reproduced. On the other hand, if the axis is oriented toward the top left, i.e., the direction is between [001] and [−100], the walls at pinning site B are reproduced. The same is true for the case that the easy axis is not parallel to the *x*-*z* plane, with the projection of the axis on the plane. Thus, these simulations demonstrated that the extrinsic magnetic anisotropy governs the correlation.

The reversal of chirality originates from the revealed anisotropy of the vortex spin structure. The structural anisotropy is intrinsic in the vortex walls since it is well reproduced by simulations neglecting anisotropy energy. The resulting difference in the spin configuration between CW and CCW vortex walls causes the simultaneous reversal of the vortex chirality and the magnetization directions of separated domains, which maintains the correlation corresponding to the strain-induced magnetic anisotropy. Understanding the mechanism of chirality formation is indispensable for controlling the chirality. The chirality is determined according to the selection rule and is dependent on the magnetization directions of separated domains and the magnetic anisotropy at the pinning sites. Magnetic anisotropy can be induced not only by crystal imperfections, which exist in all ferromagnetic nanowires and involve localized strain, but also by various external factors such as external stress. So far, intensive studies have been carried out on controlling the vortex spin configurations in nanodots or nanorings because of their potential use as memory cells, in which the chirality can represent one bit. Controlling the chirality of vortex walls will contribute to the realization of novel memory storage technologies.

In conclusion, we could visualize the in-plane anisotropic structures of vortex domain walls by Lorentz microscopy. The intrinsic structural anisotropy results in an energy difference between CW and CCW vortex walls through extrinsic magnetic anisotropy, which is induced by strain at the pinning sites; one of the two chirality forms is stabilized at each pinning site with a selection rule dependent on the magnetization directions of separated domains. The observed results proved that the simultaneous reversal of the vortex chirality and the magnetization directions takes place according to this rule.

We thank T. Asaka and X. Z. Yu for discussions. This work was partly supported by a Nanotechnology Network Project of MEXT, Japan.

*Present address: Transmission Electron Microscopy Cluster, NIMS, Tsukuba 305-0047, Japan.

[1] A. Yamaguchi *et al.*, Phys. Rev. Lett. **92**, 077205 (2004).
[2] M. Hayashi *et al.*, Phys. Rev. Lett. **97**, 207205 (2006).
[3] L. Thomas *et al.*, Nature (London) **443**, 197 (2006).
[4] M. Kläui *et al.*, Phys. Rev. Lett. **94**, 106601 (2005).
[5] G. S. D. Beach *et al.*, Nature Mater. **4**, 741 (2005).
[6] J. Raabe *et al.*, J. Appl. Phys. **88**, 4437 (2000).
[7] T. Uhlig and J. Zweck, Phys. Rev. Lett. **93**, 047203 (2004).
[8] C. Brownlie *et al.*, J. Appl. Phys. **100**, 033902 (2006).
[9] C. W. Sandweg *et al.*, J. Appl. Phys. **103**, 093906 (2008).
[10] M. Kläui *et al.*, J. Magn. Magn. Mater. **272-276**, 1631 (2004).
[11] M. Konoto *et al.*, J. Appl. Phys. **103**, 023904 (2008).
[12] M. Laufenberg *et al.*, Appl. Phys. Lett. **88**, 052507 (2006).
[13] R. D. McMichael and M. J. Donahue, IEEE Trans. Magn. **33**, 4167 (1997).
[14] K. A. Nugent *et al.*, Phys. Rev. Lett. **77**, 2961 (1996).
[15] M. Beleggia and Y. Zhu, in *Modern Techniques for Characterizing Magnetic Materials*, edited by Y. Zhu (Kluwer Academic, London, 2005), Chap. 7.
[16] H. Yamada, M. Kawasaki, and Y. Tokura, Appl. Phys. Lett. **86**, 192505 (2005).
[17] M. Izumi *et al.*, Phys. Rev. B **60**, 1211 (1999).
[18] J. M. Cowley, in *International Tables for Crystallography*, edited by A. J. C. Wilson and E. Prince (Kluwer Academic, London, 1999), Vol. C, p. 259.
[19] M. J. Donahue and D. G. Porter (http://math.nist.gov/oommf).
[20] Y. Suzuki *et al.*, J. Appl. Phys. **83**, 7064 (1998).
[21] R. Akiyama *et al.*, Appl. Phys. Lett. **79**, 4378 (2001).
[22] C. Kwon *et al.*, J. Magn. Magn. Mater. **172**, 229 (1997).